Tuning electronic properties of graphene heterostructures by amorphous-to-crystalline phase transitions

S. Kulju,[1,2,3] J. Akola,[1,2,3,*] D. Prendergast,[3] and R. O. Jones[4]

[1]*Department of Physics, Tampere University of Technology, P.O. Box 692, FI-33101 Tampere, Finland*

[2]*COMP Centre of Excellence, Department of Applied Physics, Aalto University, FI-00076 Aalto, Finland*

[3]*The Molecular Foundry, Lawrence Berkeley National Laboratory, Berkeley, California 94720, USA*

[4]*Peter Grünberg Institut PGI-1 and JARA/HPC, Forschungszentrum Jülich, D-52425 Jülich, Germany*

(Received 23 December 2015; revised manuscript received 9 March 2016; published 31 May 2016)

The remarkable ability of phase change materials (PCM) to switch between amorphous and crystalline states on a nanosecond time scale could provide new opportunities for graphene engineering. We have used density functional calculations to investigate the structures and electronic properties of heterostructures of thin amorphous and crystalline films of the PCM GeTe (16 Å thick) and $Ge_2Sb_2Te_5$ (20 Å) between graphene layers. The interaction between graphene and PCM is very weak, charge transfer is negligible, and the structures of the chalcogenide films differ little from those of bulk phases. A crystalline GeTe (111) layer induces a band gap opening of 80 meV at the Dirac point. This effect is absent for the amorphous film, but the Fermi energy shifts down along the Dirac cone by −60 meV. $Ge_2Sb_2Te_5$ shows similar features, although inherent disorder in the crystalline rocksalt structure reduces the contrast in band structure from that in the amorphous structure. These features originate in charge polarization within the crystalline films, which show electromechanical response (piezoelectricity) upon compression, and show that the electronic properties of graphene structures can be tuned by inducing ultrafast structural transitions within the chalcogenide layers. Graphene can also be used to manipulate the structural state of the PCM layer and its electronic and optical properties.

DOI: 10.1103/PhysRevB.93.195443

I. INTRODUCTION

The remarkable structural and electronic properties of graphene have led to an entirely new branch of materials science [1]. A single hexagonal graphite layer is surprisingly stable and can be wrapped into nanotubes and other structures, and its high electronic mobility makes it particularly attractive for applications in electronics. The successful preparation of graphene has also focused renewed attention on other layered materials and on intercalated compounds with unusual properties. Graphene is, moreover, the simplest example of a zero-gap semiconductor with a "Dirac cone" band structure at the Fermi energy, and this has led to poor performance in optical devices. Recent work has shown, however, that heterostructures of graphene with materials with a gap can be prepared with much improved properties [2]. Bi_2Te_3, for example, has a hexagonal structure like graphene and is a small band gap material from the "topological insulator" (TI) family. In TI materials, strong spin-orbit coupling induces surface states that are protected against time-reversal perturbations, and the band structure at the surface also shows a Dirac cone.

Bi_2Te_3 has been well studied in the context of thermoelectric applications, and thin films are topological insulators with low charge carrier concentrations and high mobility at surfaces [3]. It has been shown very recently that layers of Bi_2Te_3 and another TI material Sb_2Te_3 can be grown epitaxially on a Si(111) substrate. The result is a *p-n* junction where the chemical potential is tunable by up to 200 meV by varying the thickness of the Sb_2Te_3 layer [4]. Moreover, nanowires of Bi_2Te_3 show a reversible crystalline-amorphous phase change that can be induced by heat, laser, and electric field treatment [5], and share these properties with commercial phase change materials (PCM). PCM have been used in rewritable data recording for over 20 years [digital versatile disk (DVD-RW), Blu-ray Disc Recordable Erasable (BD-RE)], where the rapid switching between crystalline (*c*) and amorphous (*a*) forms of nanosized bits in a polycrystalline layer is monitored by changes in the resistivity or optical properties. The most common PCM are chalcogenide alloys, particularly those with compositions along the pseudobinary line $(GeTe)_{1-x}(Sb_2Te_3)_x$ (GST). Extensive experimental and theoretical studies have been carried out on GST materials, with particular focus on GeTe and $Ge_2Sb_2Te_5$ (GST-225) [6–16].

GST materials are also leading candidates for computer random access memory (PC-RAM) [17–19] and are expected to provide nonvolatile memory in future low-energy electronic devices. The phase change in PC-RAMs is initiated by resistive heating, and the state is monitored by measuring the resistivity [20]. High programming currents are incompatible with low-power operation of PC-RAM, and one way of reducing the current is to lower the heat loss at the interface between the GST layer and the heater electrode. Graphene and carbon nanotubes (CNT) are extremely good heat conductors in-plane or along the tube axis [21,22], but the weak interactions between layers lead to low out-of-plane thermal conductivity [23,24]. Reduced heat loss from the PCM layer has been demonstrated recently with carbon nanotubes [25,26] and graphene [27], where low set and reset currents were attained, and 10^5 programming cycles were achieved with graphene as an electrode interface material [27]. The interaction between the PCM and the heater (such as TiN) also leads to degradation of PC-RAM [28,29], which could well be reduced by a graphene buffer between them.

A graphene buffer could aid other applications, such as ferroelectricity in PCM [30,31]. Graphene would have

*jaakko.akola@tut.fi

advantages for a ferroelectric RAM built from GST materials (including GeTe and $Ge_2Sb_2Te_5$), since the mismatch between the (111) surface of the rocksalt type GeTe or GST-225 and $\sqrt{3} \times \sqrt{3}$ overlayer on graphene is less than 0.1 Å, so that films grown on graphene should be relatively strain-free and/or free of lateral modulation (e.g., moiré pattern). A vertical electric field can induce a band gap in a graphene bilayer, and this mechanism is the basis of a gate-controlled Re-RAM cell [32]. A density functional study of graphene/GST-225 crystalline superlattices showed that the Dirac fermions in the graphene layer are strongly affected by the GST layers [33].

These aspects have prompted us to ask whether the remarkable ultrafast phase transition of PCMs could be combined with the 2D properties of graphene. The key issues are the amorphous state of the PCM layer and its properties when introduced into a graphene heterostructure (sandwich). It is computationally challenging to model the electronic structure of amorphous systems with hundreds of atoms, and we know of no previous study of such effects. We have applied density functional (DF) methods to determine the structures and electronic properties of crystalline and amorphous thin films of GeTe (16 Å) and GST-225 (20 Å) and how they are modified when confined between graphene sheets. We show how the electronic properties of graphene are affected by the presence of the chalcogenide layers and that its conductivity can be tuned by inducing structural phase transitions in the chalcogenide layers. Conversely, graphene can be used as a thermal switch (heater) for tuning the electronic and optical properties of PCM layers. Opportunities for electronic applications in several fields are evident.

II. COMPUTATIONAL METHODS

To optimize the structures and cell dimensions in such large samples we have used the CP2K/Quickstep program package [34,35], which uses a mixed Gaussian and plane-wave basis [valence triple-zeta plus polarization (TZVP), plane wave cutoff 550 Ry]. The parametrization of Perdew, Burke, and Ernzerhof (PBE) [36] for the exchange-correlation energy has provided reliable descriptions of structural properties in many Ge/Sb/Te materials [37], and is used here. The description of the weak dispersion forces between graphene and the layers has been improved by using the DFT-D3 van der Waals corrections of Grimme *et al.* [38].

Electronic properties, projected density of states and band structures, were calculated with the Quantum ESPRESSO program [39]. The self-consistent calculations used ultrasoft pseudopotentials for all elements, a plane-wave cutoff for the orbitals of 40 Ry, and a charge density cutoff of 320 Ry. Band structure calculations, particularly for the largest heterostructure systems (*c*-GST-225, *a*-GST-225, *a*-GeTe), used the method of Shirley [40,41], where the solutions of the Kohn-Sham equations for a small number of wave vectors **k** are used to find a basis of periodic functions that best span the periodic parts of such solutions for all **k**. This basis is then used to construct a compact **k**-dependent Hamiltonian.

Graphene layers with 216 C atoms have been used in all systems, corresponding to a lateral size of ∼25.6 Å in a hexagonal supercell (the calculations were performed in a corresponding orthorhombic supercell). The GeTe heterostructures comprised 108 atoms each of Ge and Te (432 atoms in total), and 57 Ge, 58 Sb, and 144 Te for GST-225 (475 atoms in total). The crystalline GST-225 layer comprised 29 vacancies (10%) corresponding to the rocksalt phase of the bulk structure that is involved in the amorphous-to-crystalline transition.

A crystalline GeTe thin film was obtained by optimizing a thin film with (111)-surface orientation cut from the rocksalt GeTe structure. The crystalline GST-225 thin film was cut from the bulk GeTe structure, followed by random replacement of Ge atoms by Sb atoms and vacancies to give the correct composition. Amorphous thin films were cut from large amorphous blocks generated in previous studies of GeTe and GST-225 [11], taking care that the amorphous thin films had the same lateral size and number of atoms as their crystalline counterparts. The initial height of the cell was large enough to avoid compression during geometry optimization. The amorphous films and graphene were relaxed by performing Car-Parrinello molecular dynamics (30 ps at 300 K) with the CPMD program [42]. The lattice constants of graphene and the chalcogenide (111) surfaces match nearly perfectly, and both hollow and on-site alignments were tested for crystalline films. Changes in the electronic structure on changing the layer separation were monitored.

The interaction (adhesion) energy was calculated from

$$E_{ad} = E_{gr} + E_{PCM} - E_{tot}, \tag{1}$$

where E_{gr} and E_{PCM} are the energies of the isolated graphene and PCM thin films in the cell of the original system, and E_{tot} is the total energy of the sandwich structure.

The total charge density and charge transfers were calculated using the CP2K program [34]. The redistribution of electron density in PCM and graphene films upon heterostructure formation has been analyzed by calculating the electron density of the periodic heterostructure and separated films in vacuum. The densities were averaged laterally in the z

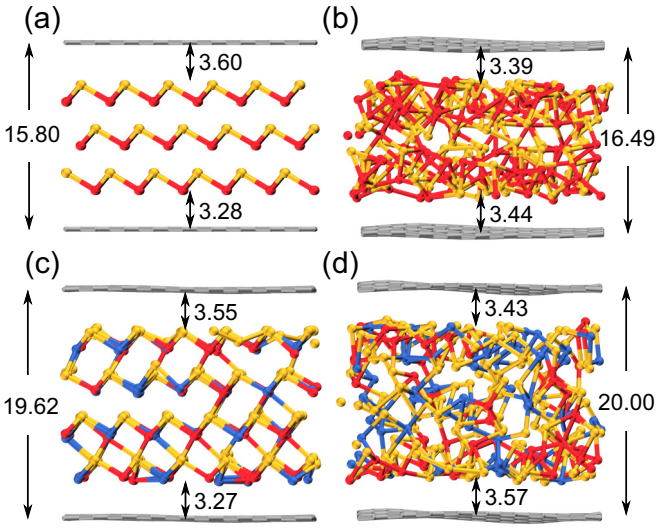

FIG. 1. Optimized geometries shown with periodic images of graphene. (a) *c*-GeTe, (b) *a*-GeTe, (c) *c*-GST, and (d) *a*-GST. Ge: red; Sb: blue; Te: yellow; C: gray. Figures are shown to scale. Measured distances are in Å.

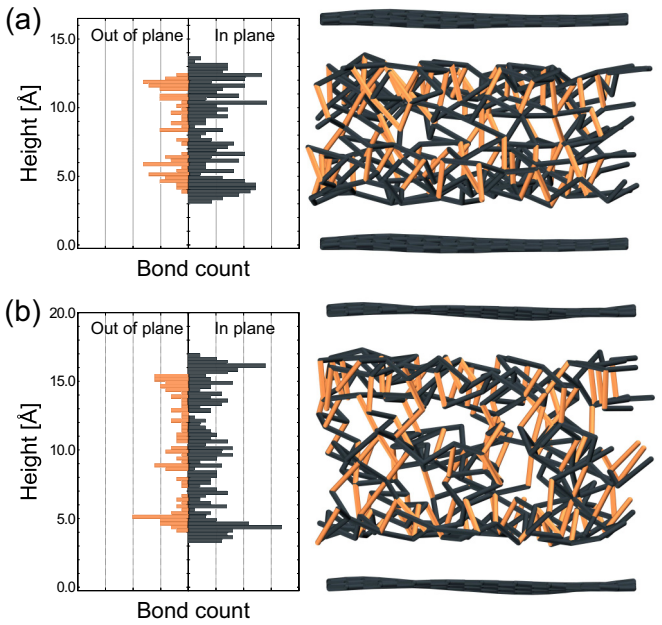

FIG. 2. In-plane (dark gray) and out-of-plane (light orange) bonds. The numbers of bonds are shown as a function of bond center height. (a) *a*-GeTe sandwich; (b) *a*-GST sandwich.

direction, and the resulting valence electron distributions of the layers were subtracted from that of the heterostructure:

$$\Delta\rho_{\perp}(z) = \rho_{\perp}^{het}(z) - \rho_{\perp}^{gr}(z) - \rho_{\perp}^{PCM}(z). \quad (2)$$

The Bader partial charge analyses for effective atomic charges [43] were performed using the code of Henkelman *et al.* [44].

III. RESULTS

The heterostructure geometries in Fig. 1 have been optimized in terms of both atomic structure and simulation cell, and the amorphous structures are based on the corresponding bulk samples which have been relaxed by (DF) molecular dynamics at 300 K before the final optimization (see Sec. II). The heterostructures show that the interaction between the PCM and graphene is very weak, and periodic boundary conditions lead to Ge–graphene–Te interfaces in the crystalline (*c*) GeTe sandwich and Ge/Sb–graphene–Te in *c*-GST [facing (111) facets of the rocksalt structure]. The interfaces are more homogeneous in amorphous systems, with a mixture of Ge/Te (Ge/Sb/Te) on both sides of the graphene layer, which forms no chemical bonds with it and follows its surface features. The asymmetry noted for crystalline films leads to different layer separations, while the amorphous films have disordered layers with lateral variations in the structure. As in the bulk amorphous structures [11,45], both PCM films have tetrahedral Ge atoms and homopolar ("wrong") bonds (Fig. S1, Supplemental Material [46]). The heterostructures are slightly thicker in the amorphous phase (4.4% and 1.9% for GeTe and GST-225, respectively), which is consistent with the observed amorphous densities in the bulk phase. The perpendicular modulation of the graphene layer is evident in the amorphous films, and vacancies at the interface in crystalline GST-225 film lead to a similar, but weaker effect.

Bonds in the amorphous material shorter than 3.2 Å were categorized by projecting them onto the XY plane ("in-plane") and Z vector ("out-of-plane") and noting the longer component. The bond sums as a function of height (Z coordinate of the bond center) are shown with the corresponding geometries in Fig. 2, which shows clear peaks for the in-plane bonds at the interfaces. The graphene sheet acts as a steric wall, and the PCM forms a layerlike structure at the interface. These layers form bonds to more randomly oriented PCM atoms below (above) that are visible as out-of-plane peaks near the PCM surface. This resembles the universal effect for liquids with hard walls [47], and is due to the weak interaction with graphene. A similar effect where surface atoms relax to their natural (covalent) coordination by forming bonds in lateral directions has been observed for an open PCM surface (vacuum) [48].

The average partial charges and their standard deviations are given in Table I. The charge is very close to zero for graphene C atoms in all cases, indicating the absence of significant charge transfer between the graphene sheet and PCM, while the values for the latter are comparable to bulk values [49]. Ge and (particularly) Sb are positively charged, and Te charges are negative. The laterally averaged charge density difference is shown for all systems in Fig. 3, which reveals a polarization effect for crystalline PCM layers, with more charge accumulating at the Ge/Sb–graphene interface. The amorphous layers induce a smaller and symmetric accumulation on both sides of graphene. We show below that this contrast between crystalline and amorphous layers is crucial for the electronic band structure.

The interfacial adhesion energies [Eq. (1), Table I] correspond to Ge–graphene–Te for *c*-GeTe, Ge/Sb–graphene–Te for *c*-GST, and mixture–graphene–mixture for the amorphous systems ("mixture" denotes Ge/Te or Ge/Sb/Te, respectively). Crystalline GeTe has ideal surfaces and the highest adhesion energy. The presence of randomly distributed vacancies and

TABLE I. Average partial charges (Bader method) and their standard deviations for the heterostructures. Last column: adhesion energy between the graphene sheet and PCM film.

		Partial charges (e)				Adhesion energy
		C	Ge	Sb	Te	(J/m^2)
GeTe	Crystalline	0.00 ± 0.03	0.36 ± 0.02		-0.35 ± 0.03	0.49
	Amorphous	0.00 ± 0.05	0.33 ± 0.07		-0.32 ± 0.07	0.41
GST	Crystalline	0.00 ± 0.05	0.35 ± 0.05	0.44 ± 0.10	-0.31 ± 0.09	0.42
	Amorphous	0.00 ± 0.04	0.33 ± 0.08	0.38 ± 0.14	-0.28 ± 0.10	0.41

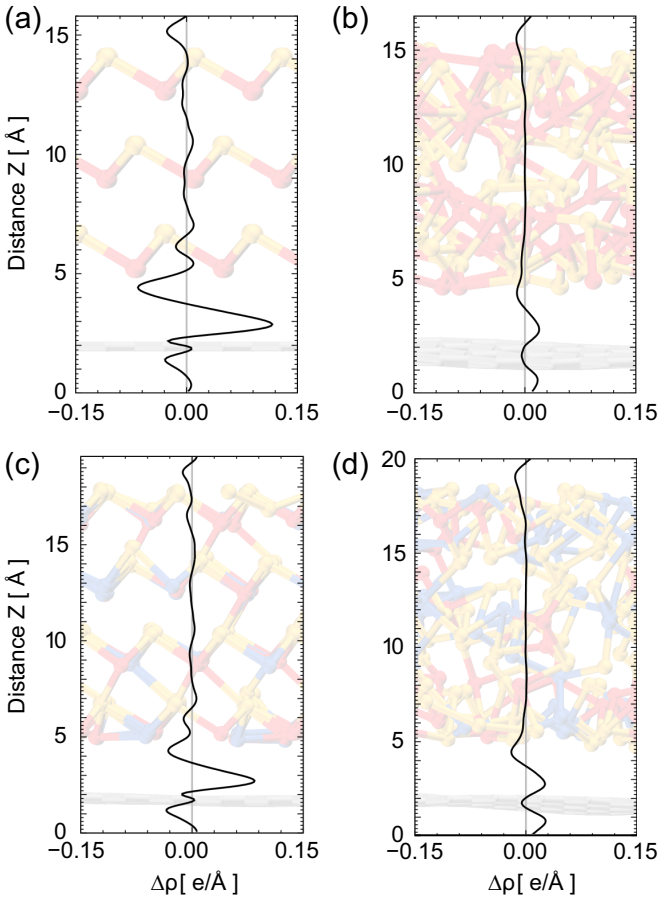

FIG. 3. Laterally averaged charge density difference for (a) c-GeTe, (b) a-GeTe, (c) c-GST, and (d) a-GST graphene heterostructures. The positive values correspond to local charge accumulation upon heterostructure formation (as compared to separated layers).

associated relaxation effects leads to structures in c-GST that are not ideal. The calculated adhesion energies are above 0.40 J/m^2 and agree reasonably well with values reported for other systems, including the Ni–graphene–Ni/Cu interface [50,51] and calculated and measured values for a graphene sheet on SiO_2 [51,52]. The importance of dispersion forces between graphene and substrate has been observed in other systems with atomically smooth surfaces [52,53].

Figure 4 shows the electronic band structure and the projected density of states (PDOS) of the c-GeTe sandwich. The band structures calculated with the method of Shirley [40] (black lines) and with a standard self-consistent calculation (dashed yellow lines) agree very well. This supports the use of the former for an improved sampling of the **k** space for PDOS calculations in systems with several hundred atoms. Furthermore, the associated computational cost per **k**-point reduces significantly with the method of Shirley.

A small band gap of the c-GeTe/graphene heterostructure is evident in both the band structure and the PDOS. The smallest hexagonal cell for the sandwich structure contains the $\sqrt{3} \times \sqrt{3}$ supercell of graphene with 30° rotation, and the K point of the graphene unit cell folds to the Γ point of the hexagonal unit cell. The graphene sheet then shows the familiar Dirac cone at Γ (see Fig. S2). The expanded view of the cone and the band structure [Fig. 4(b)] shows that the gap has opened by 80 meV, so that the system is also semiconducting in the lateral dimension. A similar effect has been observed when graphene shares an interface with SiC [54] or BN [55]. Moreover, the GeTe film has an indirect band gap of 150 meV, and its lowest unoccupied band corresponds to the onset of the conduction band for the whole system. The presence of the graphene bands leads to valence band splitting in the GeTe film, but the absence of a shift in the Fermi level indicates no charge transfer between the graphene sheet and the PCM film, as confirmed in Table I.

The large lateral supercell of the heterostructures means that the corresponding reciprocal lattice cells are very small (Fig. S2), and the calculated electronic band structures show extensive folding and an increased number of electronic states. The crystalline GeTe sandwich is the only system with a periodic structure and is the only one that can be represented with a smaller unit cell. The band structure can also be calculated for the larger systems by applying the method of Shirley. 3D images of the band structure around the Γ point within the reduced (folded) Brillouin zone are shown

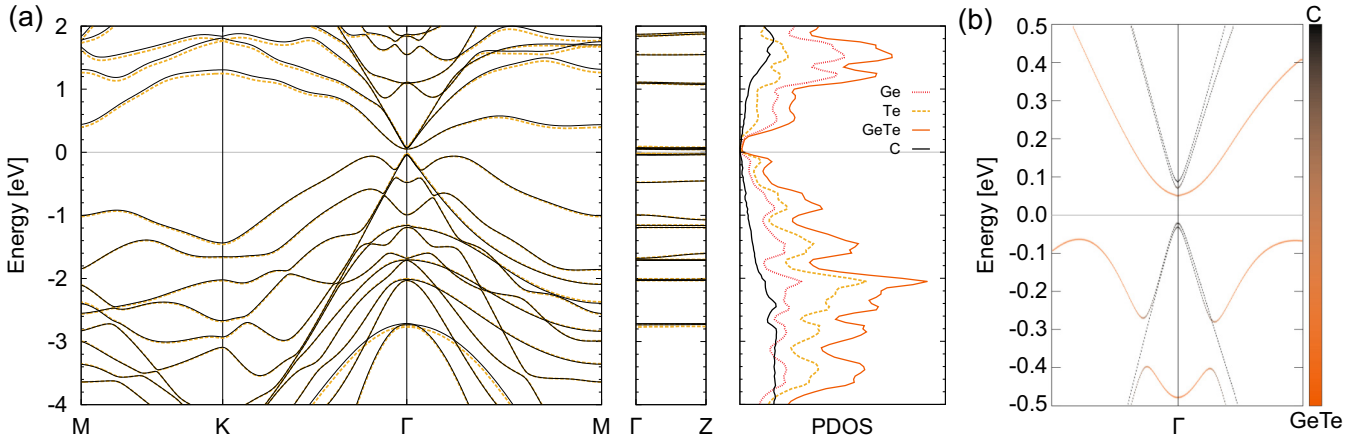

FIG. 4. Electronic band structure of the c-GeTe/graphene sandwich. (a) Band structure calculated directly (dashed yellow) and with the method of Shirley (black). The last panel shows PDOS of the same system. (b) Closeup around the Γ point with weights shows the splitting of the Dirac cone (graphene) and the indirect band gap of GeTe. The calculation is performed in the hexagonal unit cell.

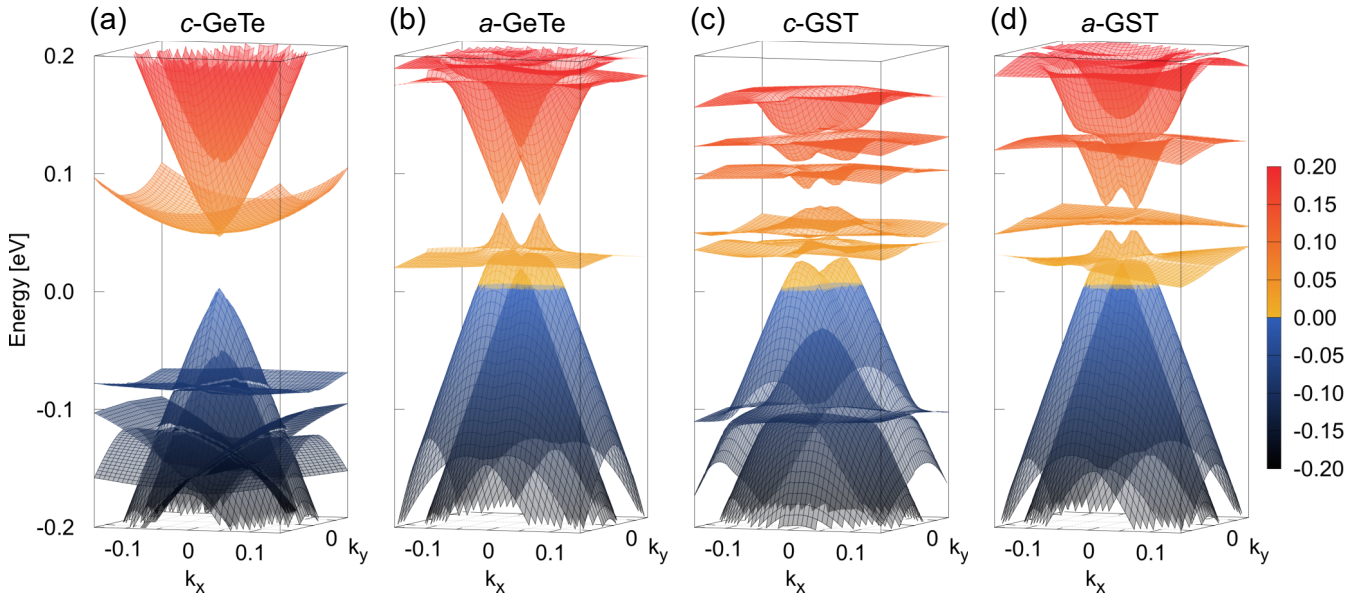

FIG. 5. Band structure near the Γ point for (a) c-GeTe sandwich, (b) a-GeTe sandwich, (c) c-GST sandwich, and (d) a-GST sandwich. The band structures were sampled with a 40 × 40 mesh within the Γ-point region, covering an area where k_x and k_y vary between −0.15 and 0.15 Å^{-1}. The Dirac cone splitting is induced (upon folding) by small variations in the cell size.

in Fig. 5 for all heterostructures, where the band structure for c-GeTe/graphene was also calculated with the (larger) supercell geometry [Fig. 1(a)] to simplify the comparison with the other systems. It is the only system where graphene does not bend, and the lateral cell is compatible with the cell size set by graphene. The graphene sheet bends in all other cases, and the lateral size of the cell changes during geometry optimization. As a result, the Dirac cones of a-GeTe, c-GST, and a-GST do not fold exactly to the Γ point, but are slightly displaced and split. The band structures were then sampled with a 40 × 40 k-point mesh. The Fermi level shifts and band gaps of graphene for all systems are given in Table II.

While the folded (and split) Dirac cones of graphene are visible near the Γ point in Fig. 5, the bands associated with PCMs are flat and can easily be identified. The impact of the particular structure of the PCM layer on the electronic structure of graphene proves interesting: crystalline films cause a band gap opening within graphene, whereas amorphous systems have little effect. In other words, one can tune the electronic properties of graphene by switching the structure (crystalline, amorphous) of the neighboring PCM layer. This is apparently due to the polarization in the asymmetric crystalline PCM films (Fig. 3), where the graphene-facing layers are different on the opposite sides, as imposed by the rocksalt structure and stoichiometry. We note that epitaxially grown GST-225 has no vacancies, and we can expect similar results as in c-GeTe.

TABLE II. Electronic band gaps of graphene and Fermi level shifts of the heterostructures. The Fermi level shift was measured from the tip of the lower cone(s); the energy gap is the minimum distance between the cone tips.

		Graphene band gap (meV)	Fermi level shift (meV)
GeTe	Crystalline	44 (80)[a]	1 (−)[a]
	Amorphous	7	−63
GST	Crystalline	18	−67
	Amorphous	7	−59

[a]Original unit cell with hexagonal symmetry.

A notable feature in the band structures is the displacement of the Fermi level. A perfect crystalline surface of GeTe has no shift, while amorphous or crystalline with defects result in shifts of ∼60 meV below the Dirac cone. The band structure of a graphene sheet from the a-GST/graphene system (Fig. S3) shows no significant opening or Fermi level shift, so that we can rule out the effect of graphene bending. The observed effects then arise mainly from the interaction between the heterostructure layers, where atomic disorder in PCM lead to local variations. Additional calculations for c-GeTe/graphene show that the graphene band gap is sensitive to the PCM alignment (on-site vs hollow site; the latter is energetically more stable) and separation of layers (Figs. S4–S8). The band gap can be opened even further by compressing the heterostructure in the perpendicular direction (piezoelectric effect).

The PDOS of large systems calculated in orthorhombic cells (Fig. 6) show distinct differences between crystalline (Fig. 4) and a-GeTe [Fig. 6(a)]. The PDOS of c-GeTe has sharp peaks, while that of a-GeTe is more uniform. The corresponding differences in GST-225 are less pronounced [Figs. 6(b) and 6(c)], and the PDOS are very similar and resemble that of a-GeTe. The structure of c-GST is less ordered than in c-GeTe, and vacancies in the former result in disorder (reduced periodic symmetry) and wrong bonds. Furthermore, the local DOS around the Fermi level of the crystalline heterostructures evolves significantly as one scans across the PCM layers, as shown in Fig. 7. In both cases, the LDOS weight shifts from the valence band to the conduction

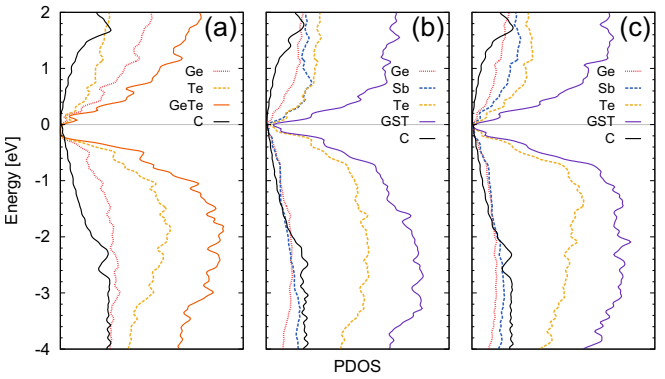

FIG. 6. Projected density of states for (a) *a*-GeTe sandwich, (b) *c*-GST sandwich, and (c) *a*-GST sandwich.

band edge once the scan proceeds towards the electron density accumulating (bottom) side. This provides further evidence that polarization within the PCM films is the origin of the graphene band gap opening.

These findings lead us to propose two types of applications based on PCM-graphene heterostructures. First, one can envisage a system of stacked PCM cells (Fig. 8), where individual cells can be manipulated by passing a heating current laterally through the contact graphene layers (RESET/SET). The state of the cells (multiple bits) could be read either optically or via perpendicular current resistivity through the heterostructure. Second, we suggest an operating principle for optoelectronic devices where laser irradiation of layers induces phase transitions (amorphous to crystalline or vice versa) and affects the lateral graphene resistance. Individual graphene layers could also be engineered by varying the PCM composition across the stack, which would also affect the optical properties. Materials along the GeTe-Sb_2Te_3 tie line, for example, show such variations, and they are used as stacked multiple recording layers in Blu-ray Discs [56,57].

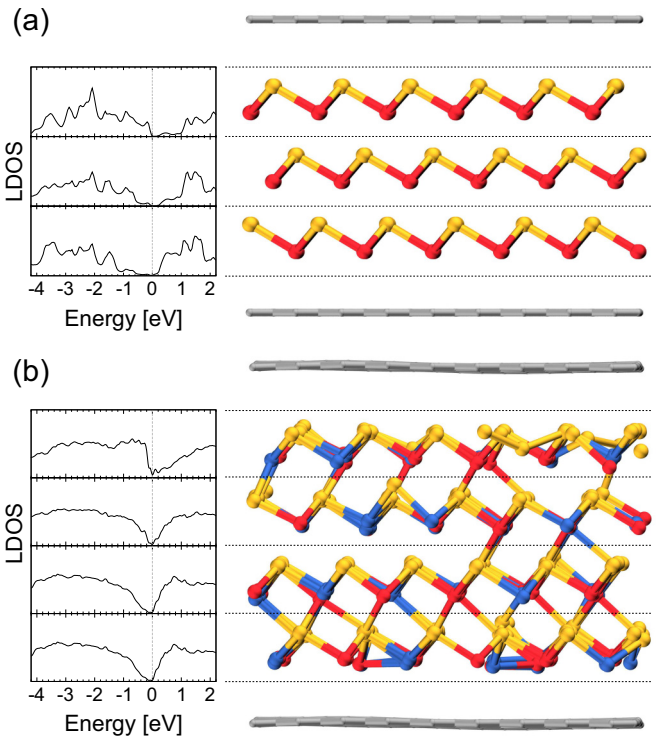

FIG. 7. Local density of states around the Fermi level for (a) *c*-GeTe and (b) *c*-GST heterostructures.

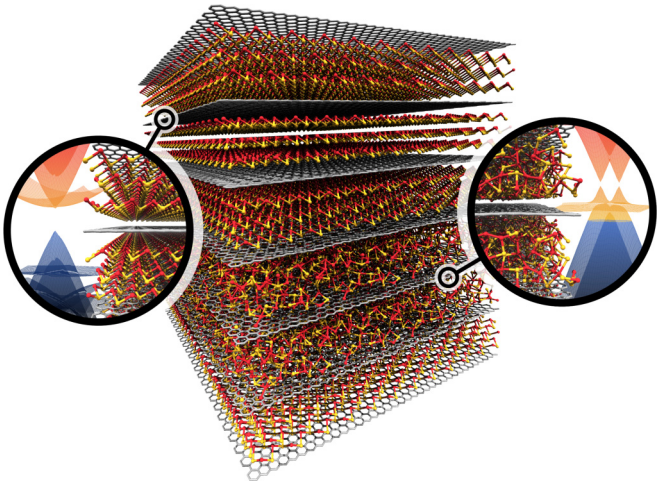

FIG. 8. Multilayer system comprising crystalline and amorphous PCM films. The "state" of the neighboring PCM films determines the electronic properties of individual graphene layers.

IV. CONCLUSIONS

DF simulations of PCM-graphene heterostructures have enabled us to study the consequences of the amorphous-to-crystalline phase transition in the PCM layers. The film thicknesses were 16 and 20 Å for GeTe and GST, respectively, and the large simulation samples (lateral dimensions of 25.6 Å) have enabled us to include effects of lateral modulation of the structure. Such simulations are computationally very challenging, since they require plausible structural models of amorphous PCM with reduced periodicity, while including a large graphene sheet (216 atoms). The task is even more challenging when extended to electronic band structure calculations, where many **k** points are needed (memory requirements) and the laterally extended system folds the Brillouin zone of graphene into a very small volume in reciprocal space with numerous electron bands. We have demonstrated the value of the method of Shirley [40,41] for carrying out non-self-consistent band structure calculations for large systems (Fig. 4).

Our initial motivation concerned two points. First, graphene can be used as a physical barrier and thermal contact component in PC-RAM and Re-RAM memory cells. Second, the chalcogenide materials are materials that are used with graphene for 2D materials engineering. We have carried out the first DF simulations of heterostructures of graphene and amorphous chalcogenide layers, as well as the corresponding crystalline heterostructures. Either component of the heterostructure can be used to manipulate the other, which opens up intriguing opportunities for future applications (Fig. 8).

The structures of PCM thin films are very similar to their bulk counterparts, with very weak interactions and charge transfer between PCM thin films and graphene. The crystalline PCMs exhibit 3+3 atomic coordination (short/long bonds) for all elements, and the alignment of rocksalt (111) facets with graphene keeps the three short bonds of the topmost layer intact. We emphasize that the lattice constants of graphene and the PCM layer match to within a few percent, which makes these systems ideal for potential 2D materials engineering. For amorphous PCM layers, the presence of an inert graphene layer leads to changes in bond orientations within the uppermost (lowermost) PCM layer as atoms form bonds in lateral directions. However, the relatively small changes in average coordination numbers indicate that the presence of a graphene interface will not alter significantly the chalcogenide structure in PC-RAM devices.

Graphene is sensitive to the crystalline state of PCM despite the weak bonds involved. This is particularly clear for *c*-GeTe, where the graphene band gap opens up (seen as separated Dirac cones in Fig. 5) and renders the system semiconducting. Further compression of the heterostructure increases the gap still further. However, the amorphous PCM film causes few changes in the graphene band structure itself, but shifts the Fermi level down by −60 meV with respect to the Dirac point, thereby enhancing the lateral conductivity. Similar Fermi level shifts are found for GST-225 films, while *c*-GST/graphene shows a small opening for the Dirac cones. The inherent disorder of the rocksalt phase (Ge/Sb/vacancy occupations of lattice sites) reduces the contrast with the amorphous GST-225 film.

Differences in the electronic properties of graphene in these systems can be traced to charge polarization within the PCM layer (Fig. 3). Sample preparation would be important, since the composition has to match with the stoichiometry (e.g., 50:50 for GeTe) to provide asymmetric crystalline films that allow polarization. The emerging opportunities based on the structural sensitivity and electromechanical response upon compression are not limited to the amorphous-to-crystalline transition, but also exist for solid-to-solid transitions, such as recently reported in the context of interfacial PCMs [58] and topological insulator heterostructures [4]. The ability to switch the polarization of the chalcogenide layer by changing the atomic structure is crucial.

ACKNOWLEDGMENTS

We are grateful for grants of computer time at CSC–IT Center for Science (Espoo, Finland), on the JUQUEEN supercomputer at the Jülich Supercomputing Centre (Forschungszentrum Jülich, Germany) from the JARA-HPC Vergabegremium (JARA-HPC partition), and on the VULCAN cluster managed by the High Performance Computing Services of the Lawrence Berkeley National Laboratory (LBNL, Berkeley, California, USA). J.A. and S.K. acknowledge financial support from the Academy of Finland through its Centres of Excellence Program (Project No. 284621). The Shirley code has been developed by D.P. at the Molecular Foundry (LBNL), supported by the Office of Science of the U.S. Department of Energy under Contract DE-AC02-05CH11231.

[1] A. K. Geim and K. S. Novoselov, Nat. Mater. **6**, 183 (2007).
[2] H. Qiao, J. Yuan, Z. Xu, C. Chen, S. Lin, Y. Wang, J. Song, Y. Liu, Q. Khan, H. Y. Hoh, C.-X. Pan, S. Li, and Q. Bao, ACS Nano **9**, 1886 (2015).
[3] K. Hoefer, C. Becker, D. Rata, J. Swanson, P. Thalmeier, and L. H. Tjeng, Proc. Natl. Acad. Sci. (U.S.A.) **111**, 14979 (2014).
[4] M. Eschbach, E. Młyńczak, J. Kellner, J. Kampmeier, M. Lanius, E. Neumann, C. Weyrich, M. Gehlmann, P. Gospodarič, S. Döring, G. Mussler, N. Demarina, M. Luysberg, G. Bihlmayer, T. Schäpers, L. Plucinski, S. Blügel, M. Morgenstern, C. M. Schneider, and D. Grützmacher, Nat. Commun. **6**, 8816 (2015).
[5] N. Han, S. I. Kim, J.-D. Yang, K. Lee, H. Sohn, H.-M. So, C. W. Ahn, and K.-H. Yoo, Adv. Mater. **23**, 1871 (2011).
[6] M. Chen, K. A. Rubin, and R. W. Barton, Appl. Phys. Lett. **49**, 502 (1986).
[7] J. Y. Raty, V. Godlevsky, P. Ghosez, C. Bichara, J. P. Gaspard, and J. R. Chelikowsky, Phys. Rev. Lett. **85**, 1950 (2000).
[8] A. V. Kolobov, P. Fons, A. I. Frenkel, A. L. Ankudinov, J. Tominaga, and T. Uruga, Nat. Mater. **3**, 703 (2004).
[9] H. Lv, P. Zhou, Y. Lin, T. Tang, B. Qiao, Y. Lai, J. Feng, B. Cai, and B. Chen, Microelectron. J. **37**, 982 (2006).
[10] M. Wuttig and N. Yamada, Nat. Mater. **6**, 824 (2007).
[11] J. Akola and R. O. Jones, Phys. Rev. B **76**, 235201 (2007); J. Phys.: Condens. Matter **20**, 465103 (2008).
[12] J. Akola, R. O. Jones, S. Kohara, S. Kimura, K. Kobayashi, M. Takata, T. Matsunaga, R. Kojima, and N. Yamada, Phys. Rev. B **80**, 020201 (2009).
[13] R. E. Simpson, M. Krbal, P. Fons, A. V. Kolobov, J. Tominaga, T. Uruga, and H. Tanida, Nano Lett. **10**, 414 (2010).
[14] J. Kalikka, J. Akola, and R. O. Jones, Phys. Rev. B **90**, 184109 (2014).
[15] J. Y. Raty, W. Zhang, J. Luckas, C. Chen, R. Mazzarello, C. Bichara, and M. Wuttig, Nat. Commun. **6**, 7467 (2015).
[16] I. Ronneberger, W. Zhang, H. Eshet, and R. Mazzarello, Adv. Funct. Mater. **25**, 6407 (2015).
[17] I.-M. Park, J.-K. Jung, S.-O. Ryu, K.-J. Choi, B.-G. Yu, Y.-B. Park, S. M. Han, and Y.-C. Joo, Thin Solid Films **517**, 848 (2008).
[18] S. Raoux, R. M. Shelby, J. Jordan-Sweet, B. Munoz, M. Salinga, Y.-C. Chen, Y.-H. Shih, E.-K. Lai, and M.-H. Lee, Microelectron. Eng. **85**, 2330 (2008).
[19] A. Pirovano, A. Redaelli, F. Pellizzer, F. Ottogalli, M. Tosi, D. Ielmini, A. L. Lacaita, and R. Bez, IEEE Trans. Device Mater. Reliab. **4**, 422 (2004).
[20] A. Pirovano, A. Lacaita, A. Benvenuti, F. Pellizzer, and R. Bez, IEEE Trans. Electron Devices **51**, 452 (2004).
[21] P. Kim, L. Shi, A. Majumdar, and P. L. McEuen, Phys. Rev. Lett. **87**, 215502 (2001).
[22] X. Xu, L. F. C. Pereira, Y. Wang, J. Wu, K. Zhang, X. Zhao, S. Bae, C. Tinh Bui, R. Xie, J. T. L. Thong, B. H. Hong, K. P. Loh, D. Donadio, B. Li, and B. Özyilmaz, Nat. Commun. **5**, 3689 (2014).
[23] V. Varshney, J. Lee, B. L. Farmer, A. A. Voevodin, and A. K. Roy, 2D Mater. **1**, 025005 (2014).

[24] E. Pop, V. Varshney, and A. K. Roy, MRS Bull. **37**, 1273 (2012).
[25] J. L. Liang, R. G. D. Jeyasingh, H.-Y. Chen, and H.-S. P. Wong, IEEE T. Electron Dev. **59**, 1155 (2012).
[26] F. Xiong, M.-H. Bae, Y. Dai, A. D. Liao, A. Behnam, E. A. Carrion, S. Hong, D. Ielmini, and E. Pop, Nano Lett. **13**, 464 (2013).
[27] C. Ahn, S. W. Fong, Y. Kim, S. Lee, A. Sood, C. M. Neumann, M. Asheghi, K. E. Goodson, E. Pop, and H.-S. P. Wong, Nano Lett. **15**, 6809 (2015).
[28] M. A. Caldwell, R. G. D. Jeyasingh, H.-S. P. Wong, and D. J. Milliron, Nanoscale **4**, 4382 (2012).
[29] C. Cabral, K. N. Chen, L. Krusin-Elbaum, and V. Deline, Appl. Phys. Lett. **90**, 051908 (2007).
[30] A. V. Kolobov, D. J. Kim, A. Giussani, P. Fons, J. Tominaga, R. Calarco, and A. Gruverman, APL Mater. **2**, 066101 (2014).
[31] J. J. Gervacio-Arciniega, E. Prokhorov, F. J. Espinoza-Beltrán, and G. Trapaga, J. Appl. Phys. **112**, 052018 (2012).
[32] H. Tian, H. Zhao, X.-F. Wang, Q.-Y. Xie, H.-Y. Chen, M. A. Mohammad, C. Li, W.-T. Mi, Z. Bie, C.-H. Yeh, Y. Yang, H.-S. P. Wong, P.-W. Chiu, and T.-L. Ren, Adv. Mater. **27**, 7766 (2015).
[33] B. Sa and Z. Sun, J. Appl. Phys. **115**, 233714 (2014).
[34] J. VandeVondele, M. Krack, F. Mohamed, M. Parrinello, T. Chassaing, and J. Hutter, Comput. Phys. Commun. **167**, 103 (2005).
[35] `http://www.cp2k.org`.
[36] J. P. Perdew, K. Burke, and M. Ernzerhof, Phys. Rev. Lett. **77**, 3865 (1996).
[37] J. Akola and R. O. Jones, Phys. Status Solidi B **249**, 1851 (2012).
[38] S. Grimme, J. Antony, S. Ehrlich, and H. Krieg, J. Chem. Phys. **132**, 154104 (2010).
[39] P. Giannozzi, S. Baroni, N. Bonini, M. Calandra, R. Car, C. Cavazzoni, D. Ceresoli, G. L. Chiarotti, M. Cococcioni, I. Dabo, A. D. Corso, S. de Gironcoli, S. Fabris, G. Fratesi, R. Gebauer, U. Gerstmann, C. Gougoussis, A. Kokalj, M. Lazzeri, L. Martin-Samos, N. Marzari, F. Mauri, R. Mazzarello, S. Paolini, A. Pasquarello, L. Paulatto, C. Sbraccia, S. Scandolo, G. Sclauzero, A. P. Seitsonen, A. Smogunov, P. Umari, and R. M. Wentzcovitch, J. Phys.: Condens. Matter **21**, 395502 (2009).
[40] E. L. Shirley, Phys. Rev. B **54**, 16464 (1996).
[41] D. Prendergast and S. G. Louie, Phys. Rev. B **80**, 235126 (2009).
[42] CPMD v3.15 ©IBM Corp. 1990-2014, ©MPI für Festkörperforschung Stuttgart 1997-2001.
[43] R. F. W. Bader, *Atoms in Molecules: A Quantum Theory* (Oxford University Press, Oxford, 1994).
[44] G. Henkelman, A. Arnaldsson, and H. Jónsson, Comput. Mater. Sci. **36**, 354 (2006); E. Sanville, S. D. Kenny, R. Smith, and G. Henkelman, J. Comput. Chem. **28**, 899 (2007); W. Tang, E. Sanville, and G. Henkelman, J. Phys.: Condens. Matter **21**, 084204 (2009).
[45] S. Caravati, M. Bernasconi, T. D. Kühne, M. Krack, and M. Parrinello, Appl. Phys. Lett. **91**, 171906 (2007).
[46] See Supplemental Material at http://link.aps.org/supplemental/10.1103/PhysRevB.93.195443 for details of the CPMD calculations, definitions of the local order parameter and occupation numbers, and tables of coordination numbers. Eight figures include local order parameters and number of wrong bonds, an explanation of the band structure folding in extended super cells, the electronic band structure with isolated graphene, together with the band structures of five film systems.
[47] R. Groot, N. Faber, and J. van der Eerden, Mol. Phys. **62**, 861 (1987).
[48] J. Akola, J. Larrucea, and R. O. Jones, Phys. Rev. B **83**, 094113 (2011).
[49] S. Gabardi, S. Caravati, M. Bernasconi, and M. Parrinello, J. Phys.: Condens. Matter **24**, 385803 (2012).
[50] J. Lahiri, T. S. Miller, A. J. Ross, L. Adamska, I. I. Oleynik, and M. Batzill, New J. Phys. **13**, 025001 (2011).
[51] Y. He, W. F. Chen, W. B. Yu, G. Ouyang, and G. W. Yang, Sci. Rep. **3**, 2660 (2013).
[52] S. P. Koenig, N. G. Boddeti, M. L. Dunn, and J. S. Bunch, Nat. Nanotechnol. **6**, 543 (2011).
[53] W. Gao, P. Xiao, G. Henkelman, K. M. Liechti, and R. Huang, J. Phys. D: Appl. Phys. **47**, 255301 (2014).
[54] S. Y. Zhou, G. H. Gweon, A. V. Fedorov, P. N. First, W. A. de Heer, D. H. Lee, F. Guinea, A. H. Castro Neto, and A. Lanzara, Nat. Mater. **6**, 770 (2007).
[55] G. Giovannetti, P. A. Khomyakov, G. Brocks, P. J. Kelly, and J. van den Brink, Phys. Rev. B **76**, 073103 (2007).
[56] T. Matsunaga, H. Morita, R. Kojima, N. Yamada, K. Kifune, Y. Kubota, Y. Tabata, J.-J. Kim, M. Kobata, E. Ikenaga, and K. Kobayashi, J. Appl. Phys. **103**, 093511 (2008).
[57] J. Akola and R. O. Jones, Phys. Rev. B **79**, 134118 (2009).
[58] R. E. Simpson, P. Fons, A. V. Kolobov, T. Fukaya, M. Krbal, T. Yagi, and J. Tominaga, Nat. Nanotechnol. **6**, 501 (2011).